photonics

MDPI

Article

# Echo-Enabled Harmonic Generation Studies for the FERMI Free-Electron Laser

**Primož Rebernik Ribič [1,*], Eléonore Roussel [1], Gregory Penn [2], Giovanni De Ninno [1,3], Luca Giannessi [1], Giuseppe Penco [1] and Enrico Allaria [1]**

1 Elettra-Sincrotrone Trieste, Strada Statale 14-km 163,5, 34149 Basovizza, Trieste, Italy; eleonore.roussel@elettra.eu (E.R.); giovanni.deninno@elettra.eu (G.D.N.); luca.giannessi@elettra.eu (L.G.); giuseppe.penco@elettra.eu (G.P.); enrico.allaria@elettra.eu (E.A.)

2 Lawrence Berkeley National Laboratory, Berkeley, CA 94720, USA; gepenn@lbl.gov

3 Laboratory of Quantum Optics, University of Nova Gorica, 5001 Nova Gorica, Slovenia

* Correspondence: primoz.rebernik@elettra.eu; Tel.: +39-403-75-8981

Received: 6 February 2017; Accepted: 8 March 2017; Published: 14 March 2017

**Abstract:** Studying ultrafast processes on the nanoscale with element specificity requires a powerful femtosecond source of tunable extreme-ultraviolet (XUV) or x-ray radiation, such as a free-electron laser (FEL). Current efforts in FEL development are aimed at improving the wavelength tunability and multicolor operation, which will potentially lead to the development of new characterization techniques offering a higher chemical sensitivity and improved spatial resolution. One of the most promising approaches is the echo-enabled harmonic generation (EEHG), where two external seed lasers are used to precisely control the spectro-temporal properties of the FEL pulse. Here, we study the expected performance of EEHG at the FERMI FEL, using numerical simulations. We show that, by employing the existing FERMI layout with minor modifications, the EEHG scheme will be able to produce gigawatt peak-power pulses at wavelengths as short as 5 nm. We discuss some possible detrimental effects that may affect the performance of EEHG and compare the results to the existing double-stage FEL cascade, currently in operation at FERMI. Finally, our simulations show that, after substantial machine upgrades, EEHG has the potential to deliver coherent multicolor pulses reaching wavelengths as short as 3 nm, enabling x-ray pump–x-ray probe experiments in the water window.

**Keywords:** free-electron laser; harmonic up-conversion; high-harmonic generation; seeding; x-ray; pump-probe; microbunching instability

## 1. Introduction

A number of recently developed or emerging sample characterization techniques, such as coherent diffraction imaging [1,2], femtosecond nanocrystallography [3], or double core-hole spectroscopy [4], require a photon source that is capable of delivering intense (gigawatt-GW peak power), coherent femtosecond pulses at wavelengths in the extreme-ultraviolet (XUV) or x-ray spectral region. At present, free-electron lasers (FELs), which amplify the light emitted by relativistic electrons wiggling inside a periodic magnetic field of an undulator [5], are the only light sources able to generate such pulses [6–9]. To study femtosecond dynamics with element sensitivity using a resonant pump-resonant probe approach [10] or a nonlinear wave-mixing scheme [11], the light source has to meet even more stringent requirements. Ideally, a FEL should produce tunable, multicolor, near transform-limited pulses, with a controlled delay, and in the best case, precisely adjustable phase profiles [12,13].

Recently, a significant effort has been devoted to improving the spectral properties, pulse tunability, and multipulse operation in FELs based on self-amplified spontaneous emission (SASE), where the amplification of light is triggered by spontaneous emission in an undulator [14]. The relatively large bandwidth of the noisy SASE spectrum can be reduced using a self-seeding scheme,

where light from the first half of the undulator is used to seed the second half, after having passed through a monochromator. This approach has been successful for improving the spectral brightness of SASE pulses, both in the hard and soft x-ray spectral regions [15,16]. Double-pulse schemes have been developed for SASE FELs that provide high-intensity two-color pulses with a variable pulse delay and flexible color separation [17–19]. These schemes, however, might suffer from stability issues related to the intrinsically noisy SASE start-up.

The limitations of the SASE scheme can be overcome by using an external seed to trigger the FEL amplification process. One option is direct seeding with a coherent source, based on high-harmonic generation (HHG) in gas [20–22]. However, this approach is still under development and is currently limited to wavelengths above several tens of nanometers, due to the relatively low efficiency of HHG. To reach shorter wavelengths, a frequency up-conversion technique such as high-gain harmonic generation (HGHG) is usually employed [23]. In HGHG (see Figure 1a, top), a seed laser imprints a periodic energy modulation at the seed wavelength $\lambda_s$ (typically in the UV) onto a relativistic electron beam (e-beam) in the modulator. After the e-beam passes through a dispersive section (a four-dipole magnet chicane), the energy modulation is converted into a current density modulation, with Fourier components spanning many harmonics of the seed. Such a microbunched e-beam emits coherent light at $\lambda_s/n$ ($n$ integer) in the XUV as the electrons traverse the periodic magnetic field of the radiator. Besides having the potential to produce fully coherent, transform-limited pulses [24], the scheme offers a natural way to control the spectrotemporal and spatial properties of the FEL pulse, by shaping the seed [25,26]. Furthermore, fine control over the output wavelengths in double-color operation can be achieved, either by using a single seed and a strongly chirped e-beam [27], or by using two seed lasers operating at different wavelengths [28].

In HGHG, the energy modulation required to produce significant bunching at the $n$th harmonic is roughly $n$ times the initial e-beam energy spread. For high $n$, this strong energy modulation severely deteriorates the FEL gain and limits the scheme to $n_{max}$~15 (to wavelengths around 15–20 nm) [23]. To reach higher harmonics, a double stage HGHG setup based on the fresh bunch [29] approach can be employed (Figure 1a, bottom). The first stage generates light at a harmonic $n_1$~8–13, which is then used to seed a fresh portion of the e-beam (with the original energy spread) in the second stage. The second radiator emits light at a harmonic $n_2$~4–8 of the first stage (i.e., at harmonic $n = n_1 n_2$ of the seed). While this method can produce a reasonably stable FEL output at wavelengths down to 4 nm or less, it uses a large portion of the e-beam, therefore reducing the maneuvering space for double-pulse operation. As it is based on the original HGHG, the method is also expected to be prone to e-beam imperfections, especially at short wavelengths [30].

These drawbacks of the HGHG cascade can be overcome using the echo-enabled harmonic generation (EEHG) approach [31,32]. EEHG uses two modulating sections to generate bunching at very high harmonics (up to $n$~100). In the first modulator, the e-beam interacts with the first seed laser, as in HGHG, inducing a relatively small energy modulation. Then, after passing through a strong dispersive section, the longitudinal e-beam phase space is shredded, resulting in a finely striated pattern. This effectively decreases the initial slice energy spread and prepares the e-beam to enter the second modulating section, which acts in the same way as the standard HGHG setup. However, due to a relatively small slice energy spread within the individual striations, only a moderate energy modulation is required from the second seed laser to obtain significant bunching at high harmonics. Because of the additional degree of freedom (another chicane), EEHG can, in principle, be tuned for a nearly flat radiation phase in the output pulse, with only modest constraints on the initial longitudinal e-beam phase space profile [30]. Recently, EEHG has produced significant microbunching at the 75th harmonic using a seed laser at 2400 nm [33].

At the FERMI FEL in Trieste, Italy, two HGHG schemes are currently in operation. FEL-1 is based on a single HGHG stage that can deliver stable pulses at wavelengths as short as ~20 nm [8], and can operate in the two-color mode [10,28]. FEL-2 consists of two HGHG stages and can operate at wavelengths down to 4 nm [34]; however, the double-stage design makes it difficult to fully exploit

two-color operation. Furthermore, due to the fact that the final harmonic number is the product of harmonic numbers for the individual HGHG stages (i.e., not all harmonics of the seed are allowed), the FEL wavelength tuning is limited for fixed e-beam energy, unless the seed can support operation across a broad wavelength range. The shortcomings of the HGHG cascade have sparked an initiative that is currently underway to modify the FEL-2 line so that it is able to operate in the EEHG configuration. The setup was preliminarily studied in [35] and the experiment is planned for 2018.

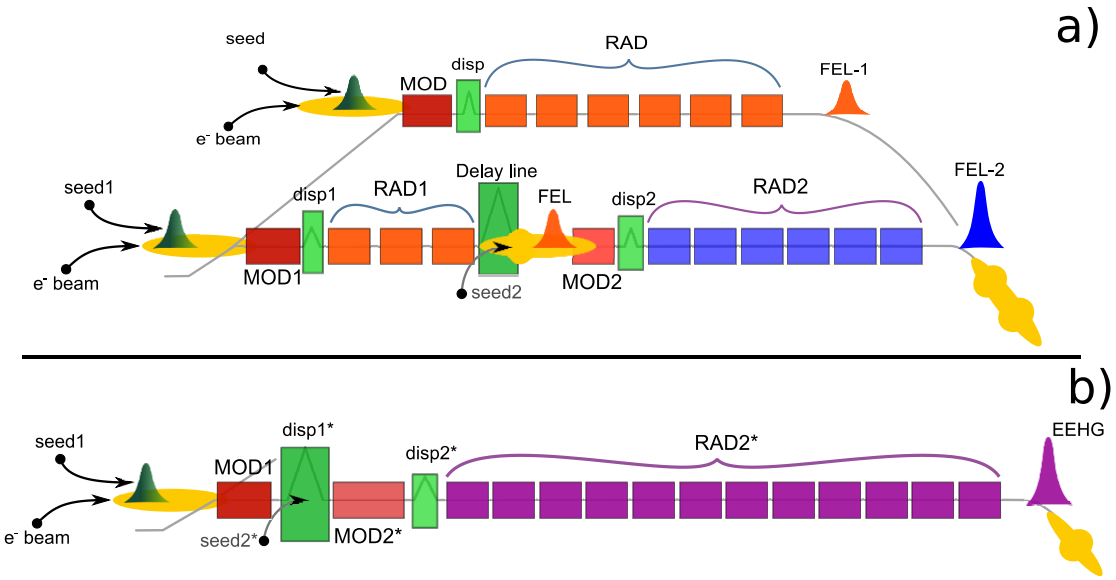


**Figure 1.** (**a**) Current FERMI layout. The top part shows the FEL-1 beamline based on the standard HGHG setup; see text for details. The seed laser, i.e., the third harmonic of a Ti:SA laser at 260 nm or an OPA, interacts with the electron bunch in the modulator (MOD). The dispersive section (disp) generates a micro-bunched e-beam that emits coherent light at one of the seed harmonics in the radiator (RAD). The beamline can produce stable FEL pulses at the GW power level and wavelengths down to 20 nm using six radiator sections with an individual length of 2.4 m. The bottom part shows the FEL-2 beamline, which is based on a two-stage HGHG cascade. In the first radiator (RAD1), coherent light is produced at a wavelength of around 20 nm (~13th harmonic of the seed). A strong chicane (delay line) is then used to delay the e-beam with respect to this light and seed a fresh portion of the electron bunch in the second modulator (MOD2). The second radiator (RAD2) then emits pulses at a harmonic (~4) of the first stage, reaching saturation at a GW power level and wavelengths around 5 nm or shorter. Currently, six radiator sections are installed, while there is space for an additional two. This beamline (with minor component modifications) will be used for the first EEHG experiment at FERMI. (**b**) Advanced EEHG layout under consideration at FERMI. The beamline will have a more compact design and up to 12 radiator sections, to ensure saturation of the output power at wavelengths around 3 nm or shorter; see text for details.

In the manuscript, we present the EEHG experimental layout suited to the FERMI FEL-2 beamline, followed by numerical simulations of the EEHG performance that can be expected in the wavelength range from 5 to 3 nm. We study the effects of the microbunching (μB) instability [36–38], which can have a significant influence on the FEL spectrum, inducing strong sidebands near the central wavelength in the worst-case scenario. The results are compared to simulations for the current performance of the two-stage HGHG cascade.

## 2. Layouts and Methods

The current layout of the two FERMI FEL beamlines is shown in Figure 1a. For the FEL-2 line (Figure 1a, bottom) to be compatible with the requirements of the EEHG scheme, a few modifications

are necessary. While the first modulator (MOD1) and the injection system for the first seed laser (seed1) can be used as is, the momentum compaction R56 (dispersive strength) of the first chicane (disp1) is not strong enough to produce a highly striated e-beam phase space, which is required for EEHG. For this purpose, we will make use of the delay line chicane, which currently serves to delay the electrons with respect to the light generated in the first stage, in order to seed a fresh part of the electron bunch in the second modulator (MOD2). Currently, the R56 of the delay line is limited to ~1 mm (1.4 GeV e-beam energy). Moving the dipole magnets further apart and upgrading the power supply will allow the dispersive strength to reach values above 2 mm, which will be sufficient to perform the first EEHG experiment at wavelengths close to 5 nm. The EEHG experiment will be carried out in a configuration where the two seed lasers have equal wavelengths. Therefore, a new, longer period (11 cm) second modulator (MOD2) will have to be installed, because the current one cannot be made resonant to an external seed at 260 nm. We will also have to design an injection system for the second laser (seed2). For this purpose, we will make use of the delay line vacuum chamber, which already has the required input ports for seed injection. No upgrades will be necessary for the second dispersive section (disp2) and the radiator line (RAD2). The gap in the first radiator (RAD1) will be fully opened (i.e., magnetic field strength set to zero) during the first EEHG experiment.

While the pilot EEHG experiment at 5.2 nm will be able to employ the existing FEL-2 beamline with minor component modifications, operation at shorter wavelengths will require a significant redesign of the layout, according to Figure 1b. We will remove the three radiator sections in the first stage (RAD1) and combine the delay line and the first dispersive section (disp1) into a single chicane (disp1*). This will make the beamline more compact and will allow the installation of additional undulators. The new radiator (RAD2*) will therefore have up to 12 sections (with a possibly smaller period for improved performance at short wavelengths), to ensure GW power levels at wavelengths around 3 nm and below. In addition, the second modulator (MOD2*) may be split into two parts, resonant to two different wavelengths. In this way, by introducing a two-color second seed (seed 2*) laser system and working in a split-radiator configuration (i.e., first few radiator sections resonant to one wavelength, while the rest are resonant to a different wavelength), the advanced EEHG layout at FERMI will enable two-color x-ray pump–x-ray probe experiments.

The e-beam parameters in the "nominal" configuration, which were used for simulations of the EEHG performances at 5.2 nm, are included in Table 1 (middle column). Such an e-beam can be routinely produced in the FERMI linear accelerator (linac). Operations at shorter wavelengths (~3 nm) will benefit from a higher peak current and e-beam energy. A peak current of 1 kA is achievable and can be obtained with the present FERMI layout by increasing the charge compression factor; the associated increased energy spread makes this option unsuitable for HGHG, but it can be used for EEHG, which is less sensitive to energy spread [30,32]. Extending the operating energy of the linac above 1.5 GeV requires an upgrade with new accelerating sections; a plan for increasing the e-beam energy up to 1.8 GeV is currently under consideration. Furthermore, to obtain significant bunching for such high harmonics ($n$~86), a major upgrade of the first chicane (disp1* in Figure 1b) will be necessary to reach dispersions in the range of 6 to 10 mm. The e-beam parameters of this "advanced configuration", which were used for simulating the EEHG performances at 3 nm, are included in the right column of Table 1.

In EEHG, the e-beam exiting the second chicane is density-modulated at a wavenumber $k = 2\pi/\lambda$, which is related to the input wavenumbers of the two seed lasers, $k_1 = 2\pi/\lambda_1$ and $k_2 = 2\pi/\lambda_2$, according to:

$$k = pk_1 + qk_2, \tag{1}$$

where $p$ and $q$ are integers. Typically, only one set ($p$, $q$) significantly contributes to the density modulation (bunching) at a given $k$ [30]. In our case, $k_1 = k_2$ and therefore $k = (p + q)k_1$, where $p + q = n$ is the harmonic number. Maximum bunching occurs for $p = -1$ [31,32]; however, this configuration requires either a strong first dispersive section (R56~8 mm, available only after a major upgrade) or a strong energy modulation from the second seed laser, to obtain significant bunching. As in the case of

HGHG for high $n$, a strong energy modulation will deteriorate the FEL gain. Therefore, during the first EEHG experiment at FERMI (using the nominal parameters from Table 1), we will work in the $p = -2$ configuration, for which values of the first R56 around 2 mm are sufficient to produce bunching of the order of 5% for $n = 50$ ($\lambda = 5.2$ nm), using only a moderate energy modulation. For simulations at 3 nm, we assumed a stronger dispersion and could therefore work at $p = -1$, allowing us to reach higher bunching compared to the $p = -2$ case.

**Table 1.** Typical EEHG operating parameters in the nominal (middle column) and advanced (right column) configurations.

| Parameter | Nominal Configuration | Advanced Configuration |
|---|---|---|
| e-beam peak current $I$ (A) | 700 | 1000 |
| e-beam energy $E$ (GeV) | 1.4 | 1.8 |
| slice energy spread $\sigma_E$ (keV) | 150 | 250 |
| emittance $\varepsilon$ (mm mrad) | 1 | 1 |
| e-beam size (μm) | 70 | 70 |
| 1st R56 (mm) | 2.1 | 8 |
| 2nd R56 (μm) | 74 | 85 |
| 1st seed peak power (MW) | 10.7 | 10.7 |
| 1st energy modulation (keV) | 450 | 450 |
| 2nd seed peak power (MW) | 135 | 151 |
| 2nd energy modulation (keV) | 824 | 868 |

In all cases, EEHG was first optimized for maximum bunching using the equations in Ref. [32]. The first and second modulators were resonant to 260 nm and had a length (period) of 3 m (10 cm) and 1.54 m (11 cm), respectively. Both seeds had a waist size of 500 μm. The first seed laser power was set for an energy modulation equal to 450 keV, while for the first chicane, we chose R56 = 2.1 mm (nominal configuration, $\lambda = 5.2$ nm) or R56 = 8 mm (advanced configuration, $\lambda = 3$ nm). The free parameters were the second chicane strength and the second seed power, which were set to optimize the bunching at the radiator entrance. The final optimization of the parameter space was carried out using time-independent FEL simulations (simulating only a single slice of the e-beam with a length $\lambda_1$) with GENESIS [39] and GINGER [40] FEL codes. The optimized EEHG parameters for both the nominal and advanced configurations are listed in Table 1.

The performance of the EEHG scheme at 5.2 nm was evaluated by carrying out time-dependent FEL simulations. The e-beam current, energy, and energy spread profiles at the end of the FERMI linac (just before the first modulator) were obtained using the particle tracking code ELEGANT [41], which takes into account collective effects such as longitudinal space charge (LSC) and coherent synchrotron radiation (CSR), which grow in bunch compressors and are at the origin of the μB instability. As the input we used the e-beam at the exit of the electron gun, generated with the General Particle Tracer (GPT) [42] package.

Additional FEL simulations were performed with electron beams whose energy profile was modified with a superposed periodic modulation at 5 μm and two different modulating amplitudes (50 keV or 100 keV). Such energy-modulated e-beams were used to study the effects of possible strong μB instabilities, that might result, e.g., from residual modulations in the photoinjector laser longitudinal profile, and to test the robustness of EEHG within the optimized parameter space of Table 1. Comparing the sensitivity of EEHG and HGHG to a controlled, periodic modulation is also important, because it can be experimentally studied by exploiting the possibility to induce periodic long wavelength modulations onto the e-beam with the laser heater available at FERMI [43,44].

For all EEHG simulations, an external script was used to reshuffle the macroparticles leaving the first dispersive section [45]. This allowed taking into account the fact that the large dispersion of the strong chicane can convert long wavelength energy modulations into current modulations. An external script was employed because the versions of the FEL codes that were used for simulations

use a "quasi-static" approximation and do not correctly take into account the motion of macroparticles over lengths longer than the seed wavelength.

Both seed laser peak powers were the same as in the time-independent case (for optimizing the bunching at the radiator entrance), and the pulses had a Gaussian shape with a full width at a half maximum (FWHM) duration of 100 fs.

For EEHG simulations at 5.2 nm, the layout of the FEL-2 beamline was used, where the magnetic field in the first radiator section (RAD1) was set to zero, i.e., these radiators only served as a drift section. The second modulator period and the dispersive strength of the delay line were modified according to Table 2 below, while the R56 of the first chicane (disp1) was set to zero.

**Table 2.** Upgrades of the FEL-2 beamline planned for the EEHG experiment at 5.2 nm.

| Parameter | Current | Modified |
|---|---|---|
| 2nd modulator period (mm) | 55 | 110 |
| 2nd modulator length (m) | 2.42 | 1.54 |
| delay line R56 (mm) | 1 | 2.1 |

For simulations of the HGHG cascade currently running at FERMI, the first stage radiation at $n_1 = 10$ was used to seed the second stage, operating at $n_2 = 5$. The first and second dispersive strengths were set to 14 μm and 8.7 μm, respectively, while the seed (260 nm) was a Gaussian pulse with a FWHM of 100 fs and peak power of 130 MW; sufficient for producing 20 MW peak power pulses at 26 nm from the first stage, that were then used to seed the second stage, generating light at 5.2 nm.

The expected performance of the EEHG scheme at shorter wavelengths (3 nm) was evaluated by carrying out time-independent simulations using e-beam parameters for the advanced configuration, as reported in Table 1.

## 3. Results and Discussion

### *3.1. The 5.2 nm Case*

The typical electron bunch length obtained with ELEGANT (using GPT as the input) was close to 1 ps. Figure 2 shows two different e-beam energy profiles (energy vs. position in the e-beam) for the central 400 fs part of the electron bunch (flat current profile), which were used in FEL simulations for the $\lambda = 5.2$ nm case. The profile given by ELEGANT (solid blue line) is characterized by a quadratic energy chirp (~14 MeV/ps$^2$), induced by longitudinal wake-fields during acceleration in the FERMI linac, and also contains energy modulations on a scale of a few or a few tens of femtoseconds (few microns), with amplitudes in the 10 keV range. They originate from a strong modulation at around 100 μm (roughly 10 μm after compression in the FERMI linac bunch compressor), present in the e-beam at the exit of the electron gun, which is then amplified by LSC and CSR. Even though there are indications suggesting that the initial modulations at the gun may be slightly overestimated due to numerical noise [46], the amplification of such modulations due to the μB instability cannot be ruled out in the actual FERMI linac. The ELEGANT profile (solid blue line) can be considered as an upper limit for the level of modulations characteristic for the FERMI e-beam, in the typical conditions used for the planned experiment.

The dashed red line profile in Figure 2 was obtained by applying a smoothing algorithm to the "elegant" profile (preserving the quadratic chirp), followed by modulating the beam with a period of 17 fs (5 μm) and an amplitude of 50 keV. Such energy modulated e-beams, with different modulating amplitudes (50 keV and 100 keV), were used to compare the performance of EEHG and the double-stage HGHG cascade in a worst-case scenario, where the energy modulation associated with the μB instability becomes comparable to the e-beam slice energy spread, and may significantly affect the FEL output, producing strong sidebands in the FEL spectra, as shown in the following (and as already

observed in experiments at the FEL-2 beamline). The same comparison can be made experimentally, thanks to the possibility of externally inducing periodic modulations into the e-beam [43].

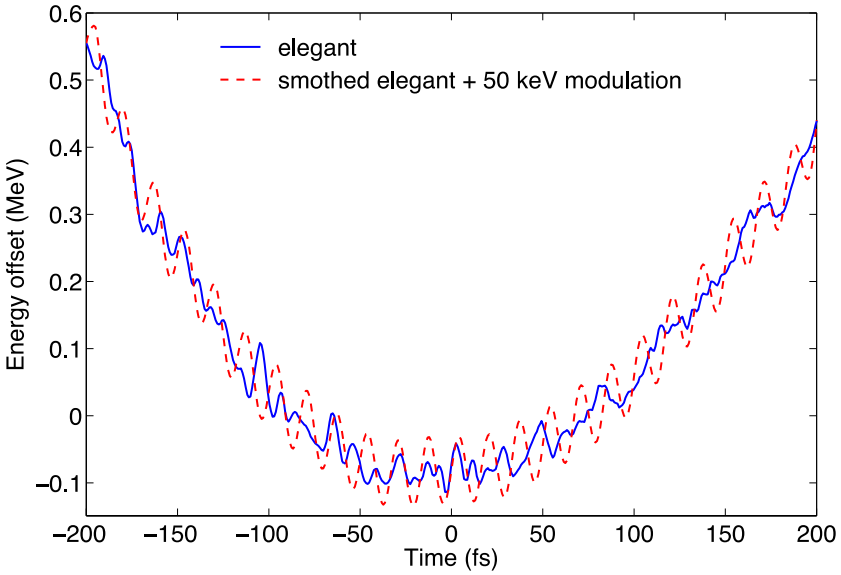


**Figure 2.** Two e-beam energy profiles used for FEL simulations. The energy offset is measured with respect to the nominal energy of 1.4 GeV.

The FEL simulation results comparing the EEHG and the double-stage HGHG schemes are presented in Figure 3. The first row shows the power profiles (Figure 3a) and the spectra (Figure 3b) of the FEL output, obtained with the optimized parameters from Table 1 (nominal configuration) and the continuous e-beam energy profile from Figure 2. For both EEHG and HGHG, saturation of the FEL power at the GW level is obtained after six radiator sections (the current FEL-2 layout, Figure 1a bottom), which shows that the two setups are comparable in performance. The pulse duration and the spectral width are similar for both schemes. Fitting a Gaussian envelope to both the power and the spectral profiles in the case of EEHG, gives $\Delta t \approx 35$ fs and $\Delta\omega \approx 1.6 \times 10^{13}$ s$^{-1}$ ($\Delta\lambda \approx 1.4 \times 10^{-3}$ nm) for the FWHM values. According to theory [47,48], the FEL pulse duration obtained by considering the width of the bunching envelope is $\Delta t = (7/6)n^{-1/3}\Delta t_{\text{seed}} \approx 31.5$ fs (27 fs). The observed pulse lengthening (35 fs vs. 31.5 or 27 fs) may be explained by the slippage effect [14], and by the fact that the bunching envelope can be altered during amplification in the radiator. It is worth stressing that the simulated HGHG performance is in good agreement with experimental results obtained at FERMI (not shown here). The time bandwidth product $\Delta t\Delta\omega \approx 0.56$ is close to the Fourier limit (0.44 for a Gaussian pulse), confirming that the spectral width mainly comes from the pulse duration. The additional broadening is a result of the non-flat (quadratic) e-beam energy profile, contaminated with instabilities. This also explains the somewhat spiky structures in the pulse temporal profiles. For both EEHG and HGHG, one can also notice the presence of a SASE background in the spectra, outside the main peaks. This background is more evident for EEHG, which can be explained by the stronger dispersive section used for this scheme.

The next two rows compare the performance of the two schemes in the presence of relatively strong modulations in the e-beam energy profile (dashed line in Figure 2), mimicking extreme cases of μB instability. As can be seen, the spiky structure of the pulse becomes amplified, see Figure 3c. Furthermore, the spectra shown in Figure 3d start to develop sidebands at frequencies $k \pm 2\pi/\lambda_{\text{m}}$, where $\lambda_{\text{m}} = 5$ μm is the modulation wavelength. While for the 50 keV modulation amplitude the sidebands are relatively weak, they can severely deteriorate the spectral quality at higher amplitudes, as shown for the 100 keV case in Figure 3e,f (for the 150 keV case not shown here, the sidebands dominate the spectra). What is interesting is the fact that, contrary to expectations, EEHG does not

seem to be immune to e-beam energy imperfections, and for our set of parameters, the scheme behaves similar to the double-stage HGHG cascade. According to these results, for both EEHG and the double stage HGHG, μB-induced modulations start to severely affect the spectral quality for amplitudes that are comparable with the e-beam energy spread (although EEHG shows a more robust behavior and the sidebands are less pronounced).

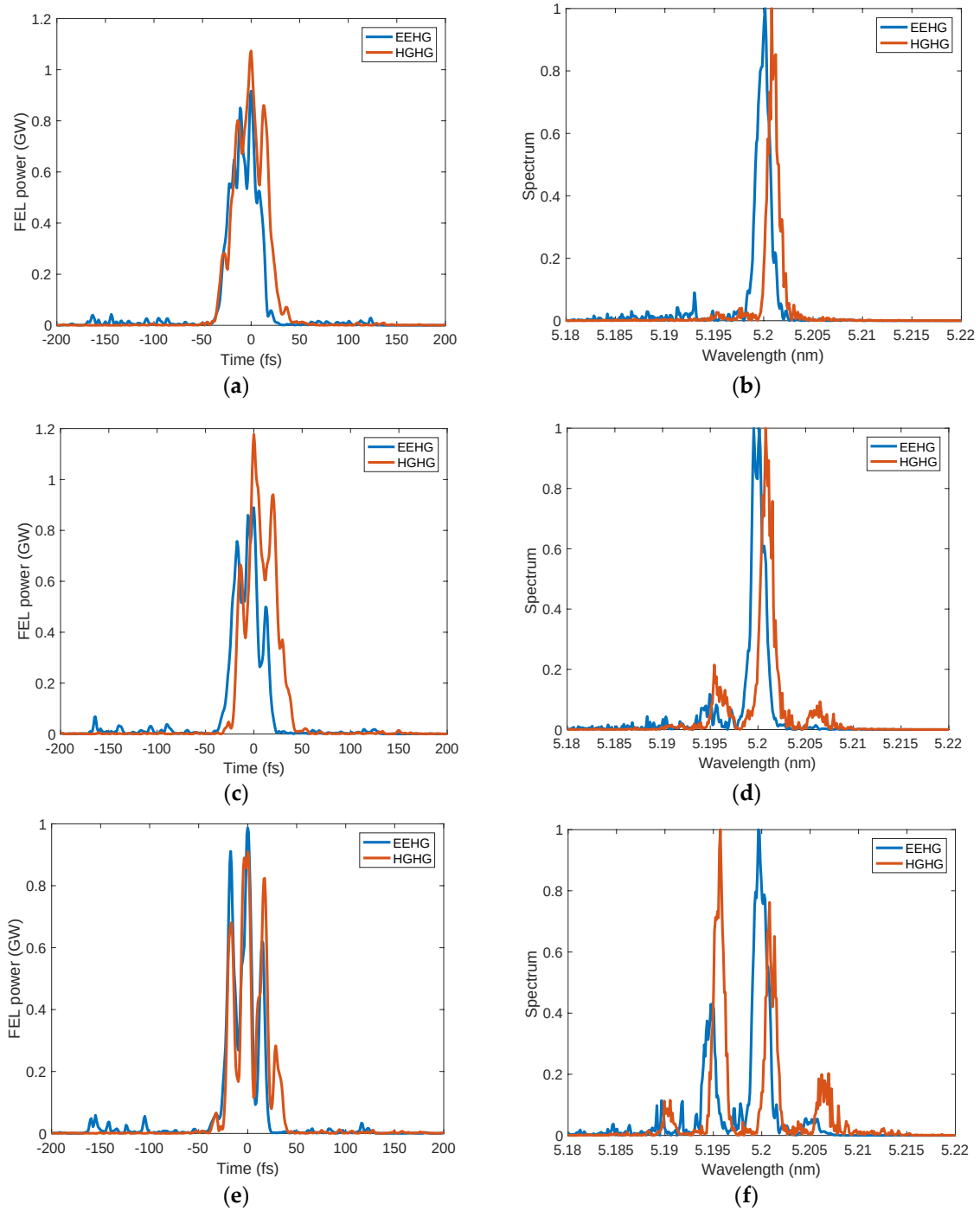


**Figure 3.** Comparison of the EEHG and the double-stage HGHG cascade for different e-beam energy profiles. (**a**,**b**) were obtained using the continuous profile in Figure 2. (**c**,**d**) are simulations results for an e-beam modulated at 5 μm with a 50 keV amplitude (Figure 2, dashed profile). In (**e**,**f**), the modulation amplitude was increased to 100 keV. The spectra in the right column are normalized to the central peak for each FEL scheme.

Several previous analyses [30,49,50] showed that, due to the highly non-linear phase space manipulations in EEHG, the bunching should be almost insensitive to the phase space imperfections, such as those shown in Figure 2. The studies assumed that the FEL spectrum is mainly affected by phase modulations in the complex bunching parameter, which determines the properties of the initial radiation (in the first part of the radiator) [30]. In our case, additional factors may be involved in the mechanism behind the sideband formation. For example, the strong dispersive section may transform the initial energy modulation into a strong current density oscillation (with the periodicity matched to that of the energy modulation), depending on the FEL parameters. Figure 4 shows the current for the case of the dashed profile of Figure 2, at the exit of the first chicane. In this case, the oscillations can reach 12% of the average current, while for a 100 keV modulation, they are increased by up to 20%. These oscillation amplitudes are in good agreement with analytical calculations of the bunching factors at the 5 μm modulation wavelength ($b = \exp[-(1/2)(2\pi/\lambda_m R_{56}(\sigma_E/E))^2]\, J_1[(2\pi/\lambda_m R_{56}(\Delta_E/E)]$, where $\Delta E$ is the modulation amplitude), which give 4.5% and 9%, respectively, for the 50 and 100 keV cases (note that the density modulation amplitude is defined as twice the value of the bunching factor).

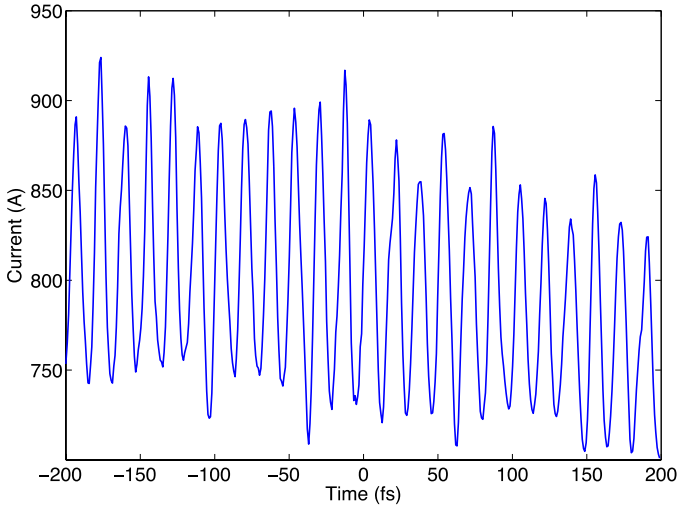


**Figure 4.** Current oscillations for the case of the dashed energy profile from Figure 2, after the e-beam passes through the strong dispersive section.

Due to the current oscillations, the FEL gain, which is proportional to $I^{1/3}$ [51], varies along the e-beam. This results in a modulation of the radiation power, clearly observed in Figure 3c,e. For the 100 keV case, the modulation period (between 15 and 18 fs) almost exactly corresponds to the modulation periods in the e-beam current and energy profiles (17 fs). As a consequence of these current and energy modulations, strong sidebands may be developed in the FEL spectrum. The details of this mechanism were recently discussed in [52]. Based on this effect, the generation of multicolor FEL pulses has recently been demonstrated, using the capability of the laser heater to introduce a long-wavelength modulation onto the e-beam energy profile [43].

Although the sensitivity of the two schemes to the μB instability is comparable for our parameter set (i.e., in both cases, the spectra are severely deteriorated when the μB-induced energy modulation becomes comparable to the initial energy spread), the fact that EEHG can tolerate higher energy spreads [30,32] makes it possible to use a strong laser heater to wash out the energy modulations before the e-beam enters the first chicane, which converts them into current oscillations [38]. Furthermore, preliminary calculations and simulations suggest that, for a stronger first R56 (4 mm or above; available after the delay line upgrade), the bunching at the sideband frequencies can be suppressed, at least to a certain degree.

### *3.2. The 3 nm Case*

To operate the FERMI FEL in the EEHG configuration at ~3 nm ($n$ = 86), which will allow accessing the nitrogen K-edge, an R56 of ~8 mm is needed in the first chicane, to obtain sufficient bunching. The decreased FEL gain at shorter wavelengths [51] will be partly compensated for by increasing the peak current from 700 A to 1 kA. Furthermore, to ensure saturation of the FEL power, an upgrade of the FEL-2 layout will require installing additional accelerating sections in the linac to increase the e-beam energy, and/or introducing more radiator sections after the last undulator. We studied both options and the results are shown in Figure 5. For the parameters of the "advanced configuration" in Table 1, but with a lower energy of 1.5 GeV (attainable with the present FERMI linac) instead of 1.8 GeV, 10 radiator sections (four more than the current setup) are necessary to approach GW power levels. By increasing the e-beam energy to 1.8 GeV (maximum attainable energy after the upgrade), only one additional radiator section (seven in total) is required for saturation.

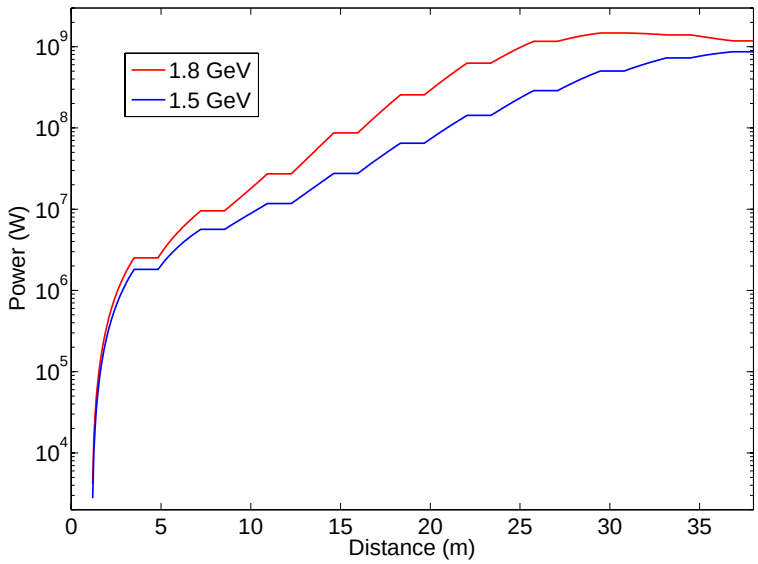


**Figure 5.** EEHG power at 3 nm as a function of the distance in the radiator. Flat regions (no increase in the power) are due to drift spaces between the radiators to accommodate e-beam focusing optics.

At this wavelength, bunching at the radiator entrance may be significantly reduced due to incoherent synchrotron radiation (ISR) and intrabeam scattering (IBS) [30,53]. However, these effects can be minimized by a proper (compact) design of the EEHG beamline and by reducing the dipole fields in the strong chicane [30].

Figure 5 shows that seven radiator sections are sufficient to reach saturation at 3 nm, using an e-beam energy of 1.8 GeV; the performance may even be improved by installing shorter period undulators. Because the advanced EEHG layout at FERMI will be able to accommodate up to 12 radiator sections, there is enough room to generate a second pulse with a different wavelength. This will enable pump-probe experiments with longitudinally (almost fully) coherent pulses in the soft x-ray spectral region at the FERMI FEL.

## 4. Conclusions

We presented the layout that will be employed at FERMI FEL for the first EEHG experiment, which is planned for 2018. The expected performance of the setup at 5.2 nm is comparable in terms of the output power and spectral quality to the double-stage HGHG cascade currently in operation. Although the EEHG scheme does not seem to show superior performance in the presence of the μB instability (for the same linac operating parameters), it still offers other advantages such as a lower sensitivity to e-spread (potentially allowing to suppress the instability) and the possibility to operate

FERMI in the double-pulse configuration at short wavelengths. For the latter, depending on the results of the preliminary experiment at 5.2 nm, we will redesign the beamline according to the scheme shown in Figure 1b. More radiator sections (and optionally more linac sections) will be added to insure saturation of the FEL power at wavelengths around 3 nm or shorter. Moreover, a combination of a split modulator and a two-color laser injection system (employing an optical parametric amplifier—OPA) will be used to ensure a flexible two-color pump-probe operation at short wavelengths. In the future, additional numerical studies will be carried out to further evaluate the impact of deleterious effects on the FEL performance, such as μB instability, IBS, and ISR, which may prove to be even more important at short wavelengths.

**Acknowledgments:** G. Penn would like to acknowledge support from the Director, Office of Science, Office of Basic Energy Sciences, of the U.S. Department of Energy under Contract No. DE-AC02-05CH11231. The authors acknowledge useful discussions with D. Castronovo, M. Danailov, S. Di Mitri, B. Diviacco, W. Fawley, M. Ferianis, B. Garcia, E. Hemsing, Z. Huang, G. Marcus, S. Spampinati, M. Veronese, and A. Zholents.

**Author Contributions:** E.A., P.R.R., G.P., and E.R. performed the simulations and analyzed the main results. P.R.R. wrote the manuscript. All authors contributed to analysis of results and manuscript improvement.

**Conflicts of Interest:** The authors declare no conflict of interest.

## References

1. Chapman, H.N.; Barty, A.; Bogan, M.J.; Boutet, S.; Frank, M.; Hau-Riege, S.P.; Marchesini, S.; Woods, B.W.; Bajt, S.; Benner, W.H.; et al. Femtosecond diffractive imaging with a soft-X-ray free-electron laser. *Nat. Phys.* **2006**, *2*, 839–843. [CrossRef]
2. Seibert, M.M.; Ekeberg, T.; Maia, F.R.N.C.; Svenda, M.; Andreasson, J.; Jonsson, O.; Odic, D.; Iwan, B.; Rocker, A.; Westphal, D.; et al. Single mimivirus particles intercepted and imaged with an X-ray laser. *Nature* **2011**, *470*, 78–81. [CrossRef] [PubMed]
3. Chapman, H.N.; Fromme, P.; Barty, A.; White, T.A.; Kirian, R.A.; Aquila, A.; Hunter, M.S.; Schulz, J.; DePonte, D.P.; Weierstall, U.; et al. Femtosecond X-ray protein nanocrystallography. *Nature* **2011**, *470*, 73–77. [CrossRef] [PubMed]
4. Berrah, N.; Fang, L.; Murphy, B.; Osipov, T.; Ueda, K.; Kukk, E.; Feifel, R.; van der Meulen, P.; Salen, P.; Schmidt, H.T.; et al. Double-core-hole spectroscopy for chemical analysis with an intense X-ray femtosecond laser. *Proc. Natl. Acad. Sci. USA* **2011**, *108*, 16912–16915. [CrossRef] [PubMed]
5. Ribic, P.R.; Margaritondo, G. Status and prospects of x-ray free-electron lasers (X-FELs): A simple presentation. *J. Phys. Appl. Phys.* **2012**, *45*, 213001. [CrossRef]
6. Ackermann, W.; Asova, G.; Ayvazyan, V.; Azima, A.; Baboi, N.; Bahr, J.; Balandin, V.; Beutner, B.; Brandt, A.; Bolzmann, A.; et al. Operation of a free-electron laser from the extreme ultraviolet to the water window. *Nat. Photon.* **2007**, *1*, 336–342. [CrossRef]
7. Emma, P.; Akre, R.; Arthur, J.; Bionta, R.; Bostedt, C.; Bozek, J.; Brachmann, A.; Bucksbaum, P.; Coffee, R.; Decker, F.-J.; et al. First lasing and operation of an angstrom-wavelength free-electron laser. *Nat. Photon.* **2010**, *4*, 641–647. [CrossRef]
8. Allaria, E.; Appio, R.; Badano, L.; Barletta, W.A.; Bassanese, S.; Biedron, S.G.; Borga, A.; Busetto, E.; Castronovo, D.; Cinquegrana, P.; et al. Highly coherent and stable pulses from the FERMI seeded free-electron laser in the extreme ultraviolet. *Nat. Photon.* **2012**, *6*, 699–704. [CrossRef]
9. Ishikawa, T.; Aoyagi, H.; Asaka, T.; Asano, Y.; Azumi, N.; Bizen, T.; Ego, H.; Fukami, K.; Fukui, T.; Furukawa, Y.; et al. A compact X-ray free-electron laser emitting in the sub-angstrom region. *Nat. Photon.* **2012**, *6*, 540–544. [CrossRef]
10. Ferrari, E.; Spezzani, C.; Fortuna, F.; Delaunay, R.; Vidal, F.; Nikolov, I.; Cinquegrana, P.; Diviacco, B.; Gauthier, D.; Penco, G.; et al. Widely tunable two-colour seeded free-electron laser source for resonant-pump resonant-probe magnetic scattering. *Nat. Commun.* **2016**, *7*, 10343. [CrossRef] [PubMed]
11. Bencivenga, F.; Cucini, R.; Capotondi, F.; Battistoni, A.; Mincigrucci, R.; Giangrisostomi, E.; Gessini, A.; Manfredda, M.; Nikolov, I.P.; Pedersoli, E.; et al. Four-wave mixing experiments with extreme ultraviolet transient gratings. *Nature* **2015**, *520*, 205–208. [CrossRef] [PubMed]

12. Prince, K.C.; Allaria, E.; Callegari, C.; Cucini, R.; De Ninno, G.; Di Mitri, S.; Diviacco, B.; Ferrari, E.; Finetti, P.; Gauthier, D.; et al. Coherent control with a short-wavelength free-electron laser. *Nat. Photon.* **2016**, *10*, 176–179. [CrossRef]
13. Gauthier, D.; Ribič, P.R.; De Ninno, G.; Allaria, E.; Cinquegrana, P.; Danailov, M.B.; Demidovich, A.; Ferrari, E.; Giannessi, L. Generation of Phase-Locked Pulses from a Seeded Free-Electron Laser. *Phys. Rev. Lett.* **2016**, *116*, 24801. [CrossRef] [PubMed]
14. Bonifacio, R.; Pellegrini, C.; Narducci, L.M. Collective instabilities and high-gain regime in a free electron laser. *Opt. Commun.* **1984**, *50*, 373–378. [CrossRef]
15. Amann, J.; Berg, W.; Blank, V.; Decker, F.-J.; Ding, Y.; Emma, P.; Feng, Y.; Frisch, J.; Fritz, D.; Hastings, J.; et al. Demonstration of self-seeding in a hard-X-ray free-electron laser. *Nat. Photon.* **2012**, *6*, 693–698. [CrossRef]
16. Ratner, D.; Abela, R.; Amann, J.; Behrens, C.; Bohler, D.; Bouchard, G.; Bostedt, C.; Boyes, M.; Chow, K.; Cocco, D.; et al. Experimental Demonstration of a Soft X-Ray Self-Seeded Free-Electron Laser. *Phys. Rev. Lett.* **2015**, *114*, 54801. [CrossRef] [PubMed]
17. Hara, T.; Inubushi, Y.; Katayama, T.; Sato, T.; Tanaka, H.; Tanaka, T.; Togashi, T.; Togawa, K.; Tono, K.; Yabashi, M.; et al. Two-colour hard X-ray free-electron laser with wide tunability. *Nat. Commun.* **2013**, *4*, 2919. [CrossRef] [PubMed]
18. Marinelli, A.; Ratner, D.; Lutman, A.A.; Turner, J.; Welch, J.; Decker, F.-J.; Loos, H.; Behrens, C.; Gilevich, S.; Miahnahri, A.A.; et al. High-intensity double-pulse X-ray free-electron laser. *Nat. Commun.* **2015**, *6*, 6369. [CrossRef] [PubMed]
19. Lutman, A.A.; Maxwell, T.J.; MacArthur, J.P.; Guetg, M.W.; Berrah, N.; Coffee, R.N.; Ding, Y.; Huang, Z.; Marinelli, A.; Moeller, S.; et al. Fresh-slice multicolour X-ray free-electron lasers. *Nat. Photon.* **2016**, *10*, 745–750. [CrossRef]
20. Lambert, G.; Hara, T.; Garzella, D.; Tanikawa, T.; Labat, M.; Carre, B.; Kitamura, H.; Shintake, T.; Bougeard, M.; Inoue, S.; et al. Injection of harmonics generated in gas in a free-electron laser providing intense and coherent extreme-ultraviolet light. *Nat. Phys.* **2008**, *4*, 296–300. [CrossRef]
21. Togashi, T.; Takahashi, E.J.; Midorikawa, K.; Aoyama, M.; Yamakawa, K.; Sato, T.; Iwasaki, A.; Owada, S.; Okino, T.; Yamanouchi, K.; et al. Extreme ultraviolet free electron laser seeded with high-order harmonic of Ti. *Opt. Express* **2011**, *19*, 317–324. [CrossRef] [PubMed]
22. Ackermann, S.; Azima, A.; Bajt, S.; Bödewadt, J.; Curbis, F.; Dachraoui, H.; Delsim-Hashemi, H.; Drescher, M.; Düsterer, S.; Faatz, B.; et al. Generation of Coherent 19- and 38-nm Radiation at a Free-Electron Laser Directly Seeded at 38 nm. *Phys. Rev. Lett.* **2013**, *111*, 114801. [CrossRef] [PubMed]
23. Yu, L.H. Generation of intense UV radiation by subharmonically seeded single-pass free-electron lasers. *Phys. Rev. A* **1991**, *44*, 5178–5193. [CrossRef] [PubMed]
24. De Ninno, G.; Gauthier, D.; Mahieu, B.; Ribič, P.R.; Allaria, E.; Cinquegrana, P.; Danailov, M.B.; Demidovich, A.; Ferrari, E.; Giannessi, L.; et al. Single-shot spectro-temporal characterization of XUV pulses from a seeded free-electron laser. *Nat. Commun.* **2015**, *6*, 8075. [CrossRef] [PubMed]
25. Gauthier, D.; Ribič, P.R.; De Ninno, G.; Allaria, E.; Cinquegrana, P.; Danailov, M.B.; Demidovich, A.; Ferrari, E.; Giannessi, L.; Mahieu, B.; et al. Spectrotemporal Shaping of Seeded Free-Electron Laser Pulses. *Phys. Rev. Lett.* **2015**, *115*, 114801. [CrossRef] [PubMed]
26. Ribič, P.R.; Gauthier, D.; De Ninno, G. Generation of Coherent Extreme-Ultraviolet Radiation Carrying Orbital Angular Momentum. *Phys. Rev. Lett.* **2014**, *112*, 203602. [CrossRef]
27. De Ninno, G.; Mahieu, B.; Allaria, E.; Giannessi, L.; Spampinati, S. Chirped Seeded Free-Electron Lasers: Self-Standing Light Sources for Two-Color Pump-Probe Experiments. *Phys. Rev. Lett.* **2013**, *110*, 64801. [CrossRef] [PubMed]
28. Allaria, E.; Bencivenga, F.; Borghes, R.; Capotondi, F.; Castronovo, D.; Charalambous, P.; Cinquegrana, P.; Danailov, M.B.; De Ninno, G.; Demidovich, A.; et al. Two-colour pump–probe experiments with a twin-pulse-seed extreme ultraviolet free-electron laser. *Nat. Commun.* **2013**, *4*, 2476. [CrossRef] [PubMed]
29. Yu, L.-H.; Ben-Zvi, I. High-gain harmonic generation of soft X-rays with the "fresh bunch" technique. *Nucl. Instrum. Methods Phys. Res. Sect. A Accel. Spectrometers Detect. Assoc. Equip.* **1997**, *393*, 96–99. [CrossRef]
30. Penn, G. Stable, coherent free-electron laser pulses using echo-enabled harmonic generation. *Phys. Rev. Spec. Top. Accel. Beams* **2014**, *17*, 110707. [CrossRef]

31. Stupakov, G. Using the Beam-Echo Effect for Generation of Short-Wavelength Radiation. *Phys. Rev. Lett.* **2009**, *102*, 74801. [CrossRef] [PubMed]
32. Xiang, D.; Stupakov, G. Echo-enabled harmonic generation free electron laser. *Phys. Rev. Spec. Top. Accel. Beams* **2009**, *12*, 30702. [CrossRef]
33. Hemsing, E.; Dunning, M.; Garcia, B.; Hast, C.; Raubenheimer, T.; Stupakov, G.; Xiang, D. Echo-enabled harmonics up to the 75th order from precisely tailored electron beams. *Nat. Photon.* **2016**, *10*, 512–515. [CrossRef]
34. Allaria, E.; Castronovo, D.; Cinquegrana, P.; Craievich, P.; Dal Forno, M.; Danailov, M.B.; D'Auria, G.; Demidovich, A.; De Ninno, G.; Di Mitri, S.; et al. Two-stage seeded soft-X-ray free-electron laser. *Nat. Photon.* **2013**, *7*, 913–918. [CrossRef]
35. Allaria, E.; De Ninno, G.; Xiang, D. Feasibility studies for single stage echo-enabled harmonic in FERMI FEL-2. In Proceedings of FEL2009, Liverpool, UK, 23–28 August 2009.
36. Borland, M.; Chae, Y.C.; Emma, P.; Lewellen, J.W.; Bharadwaj, V.; Fawley, W.M.; Krejcik, P.; Limborg, C.; Milton, S.V.; Nuhn, H.-D.; et al. Start-to-end simulation of self-amplified spontaneous emission free electron lasers from the gun through the undulator. *Nucl. Instrum. Methods Phys. Res. Sect. A Accel. Spectrometers Detect. Assoc. Equip.* **2002**, *483*, 268–272. [CrossRef]
37. Saldin, E.L.; Schneidmiller, E.A.; Yurkov, M.V. Klystron instability of a relativistic electron beam in a bunch compressor. *Nucl. Instrum. Methods Phys. Res. Sect. A Accel. Spectrometers Detect. Assoc. Equip.* **2002**, *490*, 1–8. [CrossRef]
38. Saldin, E.L.; Schneidmiller, E.A.; Yurkov, M.V. Longitudinal space charge-driven microbunching instability in the TESLA Test Facility linac. *Nucl. Instrum. Methods Phys. Res. Sect. A Accel. Spectrometers Detect. Assoc. Equip.* **2004**, *528*, 355–359. [CrossRef]
39. Reiche, S. GENESIS 1.3: A fully 3D time-dependent FEL simulation code. *Nucl. Instrum. Methods Phys. Res. Sect. A Accel. Spectrometers Detect. Assoc. Equip.* **1999**, *429*, 243–248. [CrossRef]
40. Fawley, W.M. *A User Manual for GINGER and Its Post-Processor XPLOTGIN*; Lawrence Berkeley National Laboratory: Berkeley, CA, USA, 2004.
41. Borland, M. *Elegant: A Flexible SDDS-Compliant Code for Accelerator Simulation*; Argonne National Lab.: Lemont, IL, USA, 2000.
42. De Loos, M.J.; van der Geer, S.B. General Particle Tracer: A new 3D code for accelerator and beamline design. In Proceedings of the 5th European Particle Accelerator Conference, Sitges, Spain, 10–14 Junuary 1996; p. 1241.
43. Roussel, E.; Ferrari, E.; Allaria, E.; Penco, G.; Di Mitri, S.; Veronese, M.; Danailov, M.; Gauthier, D.; Giannessi, L. Multicolor High-Gain Free-Electron Laser Driven by Seeded Microbunching Instability. *Phys. Rev. Lett.* **2015**, *115*, 214801. [CrossRef] [PubMed]
44. Spampinati, S.; Allaria, E.; Badano, L.; Bassanese, S.; Biedron, S.; Castronovo, D.; Craievich, P.; Danailov, M.B.; Demidovich, A.; De Ninno, G.; et al. Laser heater commissioning at an externally seeded free-electron laser. *Phys. Rev. Spec. Top. Accel. Beams* **2014**, *17*, 120705. [CrossRef]
45. Penn, G.; Lawrence Berkeley National Laboratory, Berkeley, CA, USA. Private Communication, 2016.
46. Borland, M. Modeling of the microbunching instability. *Phys. Rev. Spec. Top. Accel. Beams* **2008**, *11*, 30701. [CrossRef]
47. Giannessi, L.; Elettra-Sincrotrone Trieste, Trieste, Italy. Private Communication, 2016.
48. Ratner, D.; Fry, A.; Stupakov, G.; White, W. Laser phase errors in seeded free electron lasers. *Phys. Rev. Spec. Top. Accel. Beams* **2012**, *15*, 30702. [CrossRef]
49. Zhao, Z.T.; Wang, D.; Chen, J.H.; Chen, Z.H.; Deng, H.X.; Ding, J.G.; Feng, C.; Gu, Q.; Huang, M.M.; Lan, T.H.; et al. First lasing of an echo-enabled harmonic generation free-electron laser. *Nat. Photon.* **2012**, *6*, 360–363. [CrossRef]
50. Hemsing, E.; Dunning, M.; Hast, C.; Raubenheimer, T.O.; Weathersby, S.; Xiang, D. Highly coherent vacuum ultraviolet radiation at the 15th harmonic with echo-enabled harmonic generation technique. *Phys. Rev. Spec. Top. Accel. Beams* **2014**, *17*, 70702. [CrossRef]
51. Huang, Z.; Kim, K.-J. Review of x-ray free-electron laser theory. *Phys. Rev. Spec. Top. Accel. Beams* **2007**, *10*, 34801. [CrossRef]

52. Zhang, Z.; Lindberg, R.; Fawley, W.M.; Huang, Z.; Krzywinski, J.; Lutman, A.; Marcus, G.; Marinelli, A. Microbunching-instability-induced sidebands in a seeded free-electron laser. *Phys. Rev. Accel. Beams* **2016**, *19*, 50701. [CrossRef]
53. Dattoli, G.; Sabia, E. Bunching coefficients in echo-enabled harmonic generation. *Phys. Rev. Spec. Top. Accel. Beams* **2013**, *16*, 70702. [CrossRef]